https://www.scirp.org/journal/jbise
Journal of Biomedical Science and Engineering, 2026, Vol. 19, (No. 6), pp: 242-254

Design and Implementation of an Improved Exoskeleton sEMG Signal Processing System

Lijie Li, Zhe Hu, Yingshan Tian

Chongqing Bashu Secondary School, Chongqing, China

Correspondence to: Lijie Li, lijie.li.biec@bashuschool.cn; Zhe Hu, yingshan.tian.biec@bashuschool.cn
Keywords: sEMG, Signal Processing, Motion Control, Exoskeleton Finger, Rehabilitation
Received: October 31, 2025 **Accepted:** June 22, 2026 **Published:** June 25, 2026

ABSTRACT

Surface Electromyography (sEMG), the bioelectric currents generated by muscle contractions on the human body surface, enables motion control of exoskeletons. sEMG signal processing combines both software and hardware components, where accuracy and timeliness directly impact the practicality of exoskeleton motion control systems. Addressing the needs of hemiplegic patients with hand function impairments, this paper designs an improved sEMG signal processing system for exoskeleton motion control and completes the structural design and physical implementation of an exoskeleton finger. Experimental results demonstrate that the exoskeleton finger exhibits excellent adaptive capability, cooperating with human fingers to grasp various objects in daily life scenarios.

1. INTRODUCTION

Surface Electromyography (sEMG) represents the biological electrical activity produced by muscle contractions detectable on the skin surface. During voluntary movement, the nervous system generates motor commands that propagate through motor neurons, ultimately triggering action potentials at neuromuscular junctions. The summation of these action potentials forms motor unit action potentials, whose collective activity manifests as muscle contraction behavior [1]. The transmission of neural electrical signals through neurons generates action potentials that initiate muscle contractions [2]. During this process, electrical currents are generated, and electrodes placed on the skin surface detect potential differences reflecting muscular activity.

sEMG signals typically precede physical movement by 30 - 150 ms, enabling prediction of movement intention and decoding into mechanical control commands for exoskeleton applications [3, 4]. sEMG-based exoskeletons not only assist patients with limb dysfunction in rehabilitation training but also help them complete daily living activities, thereby restoring confidence [5]. The motion control technology based on sEMG signals facilitates more intelligent and humanized human-machine interaction, enhancing the

practicality and adaptability of exoskeleton equipment [6]. Given the significant social and economic value of sEMG-based exoskeletons, research on their design and implementation has become increasingly important [7].

1.1. Social Background

Globally, stroke represents a leading cause of functional impairment. In China, stroke incidence ranks first in the Asia-Pacific region, increasing at an annual rate of 8.7%. By 2030, the number of stroke cases is projected to reach 30 million, with 70% - 80% of patients experiencing varying degrees of functional impairment [8].

Functional impairment significantly affects patients' ability to reintegrate into family and society, with hand dysfunction particularly reducing quality of life [9]. Compared to lower limb walking and balance training, hand function rehabilitation presents greater challenges. Studies indicate only 15% of hemiplegic patients achieve 50% hand function recovery, and merely 3% reach 70% recovery [10]. Restoring hand function remains one of the most significant challenges for stroke patients, making improvement of hand function in hemiplegic patients an urgent priority in China [11].

1.2. Literature Review

Human study of sEMG signals dates back over 300 years. In the mid-17th century, Francesco Redi discovered that electric fish generate bioelectrical signals through muscle contraction. In 1791, Galvani confirmed the relationship between myoelectric signal generation and muscle contraction through frog muscle experiments. In 1849, DuBois-Reymond observed that human muscle contractions during movement produce bioelectrical signals. In 1944, Gasser and Erlanger received the Nobel Prize for observing electromyograms using cathode ray oscilloscopes [12].

Recent advances include:

• 2021: Khan *et al.* developed an EEG-based exoskeleton for rehabilitation therapy, demonstrating the feasibility of brain controlled assistive devices [13].

• 2022: Zhang Chi's team at Huazhong University of Science and Technology developed a pneumatic flexible supernumerary robotic limb for grasping compensation [14].

• 2012: Heo *et al.* reviewed the state of the art in hand exoskeleton technologies for rehabilitation and assistive engineering [15].

Current challenges include noise interference in sEMG acquisition (±1.5 mV amplitude) [16] and adaptive control in human-robot interaction [17]. This study addresses these challenges through a novel signal processing pipeline and underactuated mechanism design.

2. BIONIC DESIGN OF EXOSKELETON FINGER

2.1. Biomimetic Mechanism

Human hand grasping primarily relies on finger flexion. Taking the middle finger as an example, it consists of one metacarpal bone and three phalanges. The metacarpophalangeal (MP) joint connects the metacarpal and proximal phalanx, while the proximal interphalangeal (PIP) and distal interphalangeal (DIP) joints connect the phalanges. Finger flexion/extension and adduction/abduction occur in planes perpendicular and parallel to the palm, respectively [18]. Thus, the exoskeleton finger design should incorporate multiple rotating joints capable of mimicking natural finger flexion movements.

2.2. Structural Design

The proposed exoskeleton finger employs a multi joint rigid flexible bionic structure, inspired by multijoint passive elastic exoskeleton designs [19]. For easy installation and removal, a mortise-and-tenon connection mechanism allows the flexible module to slide into gaps reserved in the rigid module.

2.3. Drive Mechanism

Exoskeleton finger drive mechanisms primarily include coupling mechanisms and underactuated mechanisms. The coupling mechanism employs independent drivers and sensors for each joint, enabling precise control but with high complexity and cost. The underactuated mechanism uses a single driver to control multiple joints, achieving coordinated movement through reasonable control algorithms and transmission structures. This approach offers lower cost, simpler control, and better enveloping effects, making it more suitable for practical applications [20].

This design adopts a cable-driven underactuated structure, which offers several advantages:

- Reduced finger weight and size by eliminating direct motor connection
- High transmission efficiency through direct force conversion
- Improved device flexibility
- Lower manufacturing costs without gear transmission systems

The drive rope utilizes steel wire, a choice informed by high reliability self locking mechanisms used in in pipe robots [21].

3. DESIGN OF SEMG PROCESSING SYSTEM

3.1. sEMG Processing Flow

3.1.1. sEMG Acquisition

Common sEMG acquisition devices include patch electrodes, needle electrodes, and dry electrodes. Needle electrodes are invasive and damage skin; patch electrodes are non-invasive but complex to apply and non-reusable; dry electrodes offer non invasive measurement, convenient wearing, and reusability, analogous to the sensing integration challenges addressed in continuum robotics [22]. This study employs dry electrode acquisition devices.

3.1.2. sEMG Preprocessing

Human sEMG signals are weak and susceptible to noise, requiring preprocessing to remove equipment noise and interference signals from limb contact. The preprocessing pipeline amplifies collected signals and denoises them through filtering. The sEMG acquisition device amplifies signals, which are then sampled by Arduino at 1000 Hz and uploaded to MATLAB for processing, as shown in **Figure 1**.

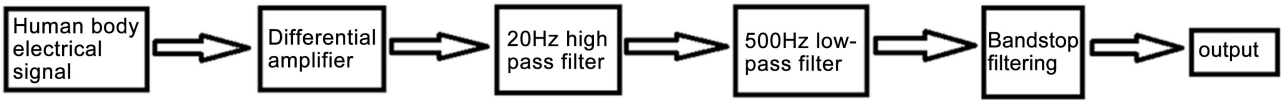

Figure 1. sEMG signal preprocessing procedure.

3.1.3. Active Segment Detection

After preprocessing, sEMG data requires labeling for subsequent classification. Manual labeling is inefficient and error-prone. This paper employs active segment detection using a dual-threshold method combining short-term energy and time-domain variance:

1) Normalize EMG data amplitude to [−1, 1]:

$$x_{\text{nom}} = \frac{x - \min(x)}{\max(x) - \min(x)} \tag{1}$$

2) Frame EMG data (300 data points per frame at 1000 Hz sampling rate)

3) Calculate frame energy:

$$E_k = \frac{1}{300}\sum_{i=1}^{300} x_i^2 \tag{2}$$

4) Calculate time-domain variance:

$$D_i = \frac{1}{w_{\text{length}}} \sum_{k=1}^{w_{\text{length}}} \left(\left| x_i(k) \right| - E_i \right)^2 \tag{3}$$

3.2. Feature Extraction and Model Training

3.2.1. Action Classification Based on Random Forest

Employing a fixed-length sliding window (N = 300 points, t = 150 points advancement) to accommodate the 300 ms lead time of sEMG signals, the system calculates features reflecting immediate signal changes [23]. Selected features include:

• **Mean Absolute Value (MAV)**: The average of the absolute values of the sEMG signal samples within a window, reflecting the overall amplitude level of the signal.

• **Integrated EMG Value (IEMG)**: The integral of the absolute value of the sEMG signal over a window, representing the total energy of the signal during the window period.

• **Time Domain Variance (VAR)**: A statistical measure reflecting the dispersion of sEMG signal samples around the mean value, indicating the stability of the signal.

• **Root Mean Square (RMS)**: The square root of the average of the squares of the sEMG signal samples, sensitive to the amplitude of the signal.

• **Average Amplitude Change (AAC)**: The average of the absolute differences between consecutive sEMG signal samples, reflecting the rate of change of the signal amplitude.

• **Short-Time Zero Crossing Rate (STZCR)**: The number of times the sEMG signal crosses zero within a window, related to the frequency characteristics of the signal.

• **Average Frequency (AF)**: The average value of the frequency components of the sEMG signal, reflecting the dominant frequency range of the signal.

• **Average Power (AP)**: The average power of the sEMG signal within a specific frequency band, indicating the energy distribution of the signal.

The three most label-correlated features (MAV, RMS, AAC) are input to a random forest classifier for handshake versus palm relaxation classification.

3.2.2. Exoskeleton Finger Control Strategy

To achieve coordinated grasping between exoskeleton and human fingers, grip force must be controlled. sEMG features reflecting muscle strength are extracted to map exoskeleton finger grip levels. Mean Absolute Value (MAV) commonly maps prosthetic hand grip strength proportionally:

$$\text{MAV} = \frac{1}{n} \sum_{i=1}^{n} |x_i| \tag{4}$$

The steering gear rotation angle is calculated as:

$$\theta_r = c \cdot \theta_M \tag{5}$$

where $\theta_M = 180^\circ$ (maximum angle), and c is a ratio factor determined by:

$$c = \begin{cases} 0 & \text{MAV} \le 0.04 \\ 0.5 & 0.04 < \text{MAV} < 0.06 \\ 1 & \text{MAV} \ge 0.06 \end{cases} \tag{6}$$

The MAV threshold values (0.04 and 0.06) were determined through a preliminary experiment involving 8 healthy subjects (4 males, 4 females, aged 22 - 35 years). Each subject performed 50 grasp-relax cycles, and the MAV values corresponding to different grip intensities (no grip, moderate grip, maximum grip) were statistically analyzed. The thresholds were set as the 25th and 75th percentiles of the MAV distribution across all trials to cover the majority of grip intensity variations. In practical applications, subject-specific

calibration is recommended: each user performs 10 - 15 grasp-relax cycles, and the thresholds are adjusted based on their individual MAV distribution to optimize grip force control accuracy.

Figure 2 illustrates the complete control flowchart.

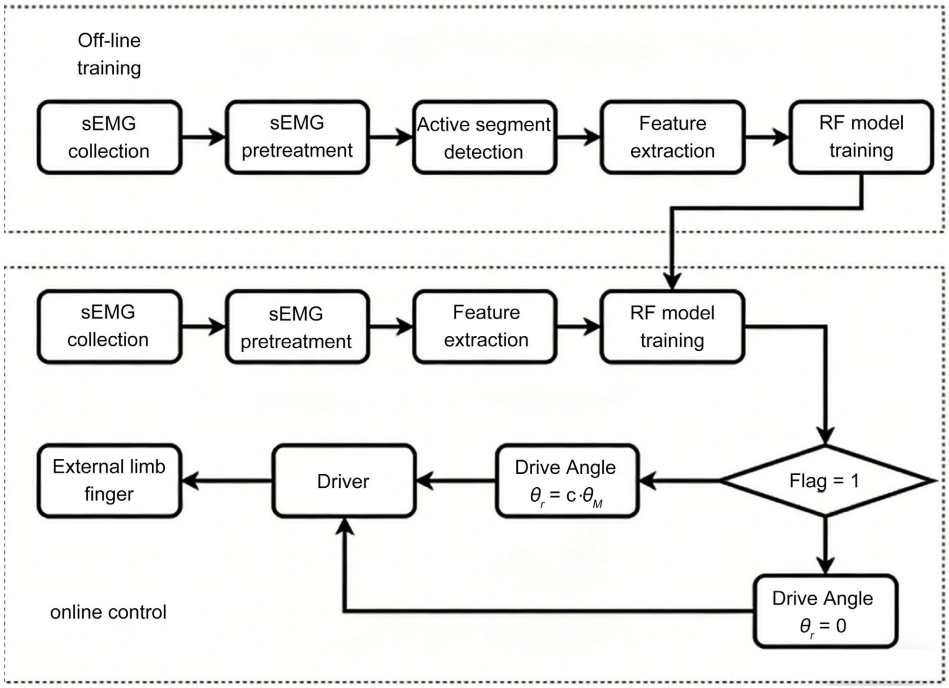

Figure 2. Exoskeleton finger control flowchart.

4. IMPLEMENTATION OF SEMG PROCESSING SYSTEM

4.1. Experimental Setup

The sEMG-based exoskeleton finger system comprises:

- Exoskeleton finger mechanical structure
- sEMG receiver
- Drive motor
- Control panel
- Upper computer
- Data processing software

Figure 3 shows the overall working process.

4.1.1. Dry Electrode

The Sizhirui dry electrode EMG sensor operates at +3.3 - 5.5 V supply voltage, outputs 0 - 3.0 V voltage, detects ±1.5 mV signals, and features PJ-342 electrode interface and XH2.54-3P module interface [22].

4.1.2. Drive Motor

A servo motor (steering engine) provides precise rotation angle control, offering small size, easy control, large torque, low cost, and light weight. Specifications: 13 kg/cm torque (6 V), 0.08 sec/60˚ speed (6 V), 3 - 7.2 V operating voltage, and 0˚ - 180˚ working angle.

4.1.3. Control Panel

Arduino UNO microcontroller with rich library functions, 14 digital I/O pins, 6 analog input pins, and 6 PWM output pins facilitates various sensor connections. Serial communication enables Arduino-upper

computer communication.

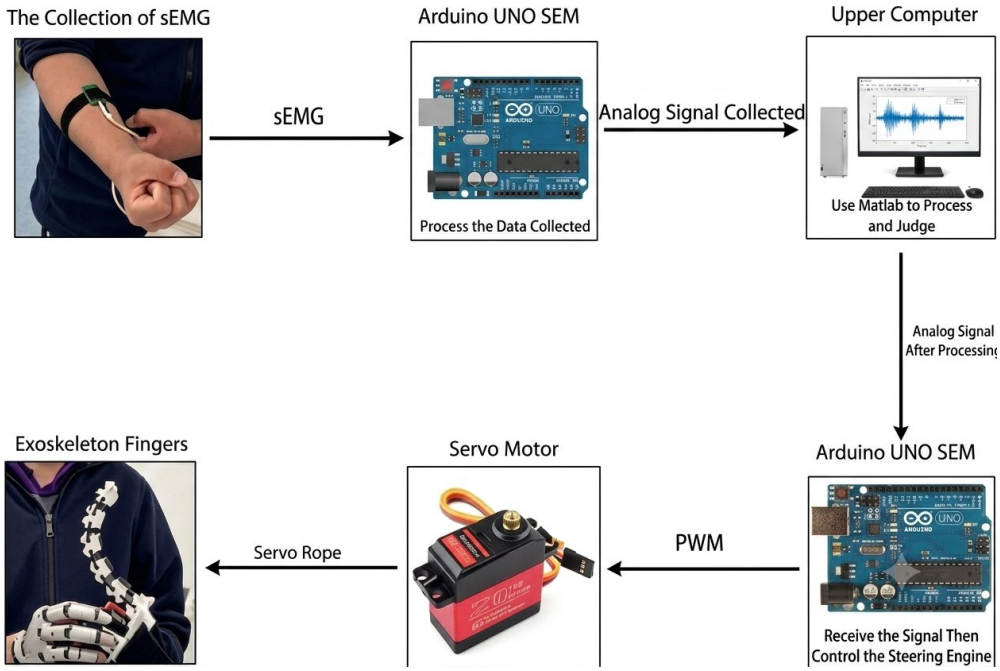

Figure 3. System overview.

4.1.4. Upper Computer

HUAWEI Matebook X Pro equipped with Intel Core Ultra9 high-performance processor (16 cores, 22 threads, 40 W power release) ensures strong computational capability and stable operation.

4.1.5. Software

MATLAB R2024a provides rapid algorithm development, mathematical/statistical/signal processing functions, complete visualization capabilities, and excellent Arduino compatibility through Simulink code generation and testing.

4.1.6. Exoskeleton Finger

The rigid-flexible coupling structure employs ABS plastic for rigid components and TPU plastic for flexible parts, manufactured via 3D printing and assembled through mortise-and-tenon joints. Figure 4 shows the physical implementation.

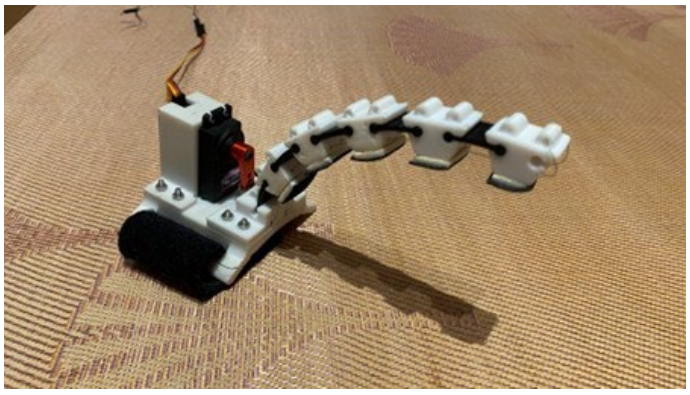

Figure 4. Exoskeleton finger physical implementation.

4.2. Experimental Process

4.2.1. Raw Data Processing

Figure 5 shows amplified data collected by the dry electrode EMG acquisition device, with horizontal axis representing collection time and vertical axis representing collected data values.

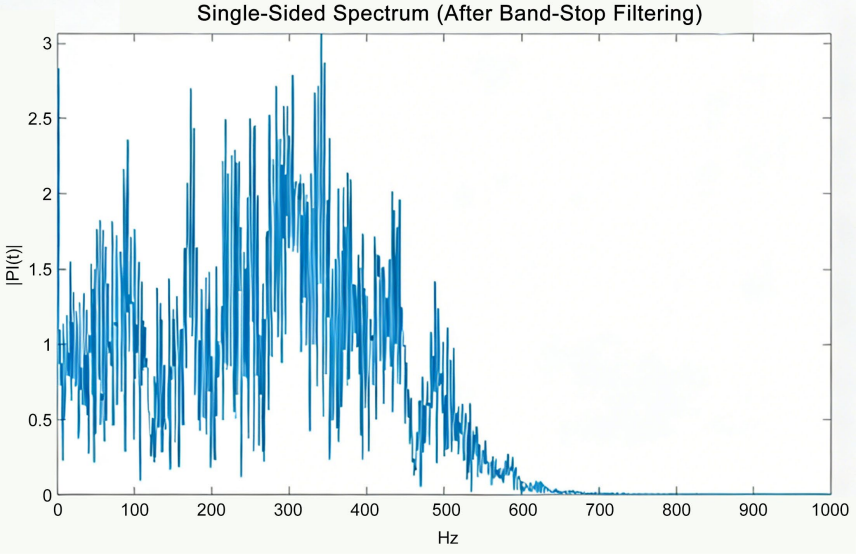

Figure 5. Raw sEMG data from different subjects.

4.2.2. Filter Denoising

Data undergoes filtering through:

- Low-pass filter (cutoff frequency: 500 Hz)
- High-pass filter (cutoff frequency: 20 Hz)
- Band-stop filter (cutoff frequency: 50 - 51 Hz)

All filters are second-order Butterworth filters. Figure 6 demonstrates effective power frequency noise removal, with sEMG energy concentrated at 20 - 200 Hz.

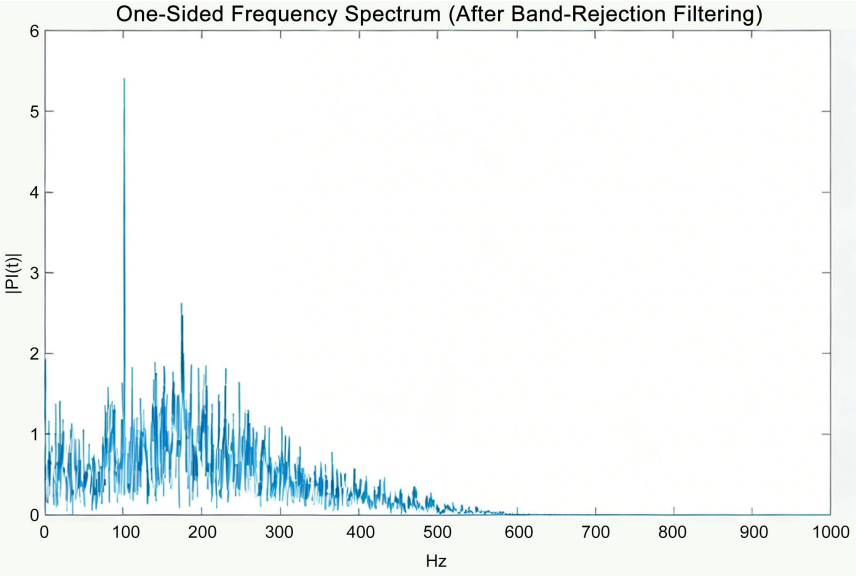

Figure 6. Filtered sEMG data.

4.2.3. Dual-Threshold Detection

To quantitatively verify the superiority of the proposed dual-threshold method (combining short-time energy and time-domain variance) in active segment detection, three methods were compared using standard performance metrics: Precision, Recall, and F1-score. The experimental data included 1000 sEMG signal segments (500 active segments and 500 non-active segments) from 10 subjects.

Table 1. Proposed dual-threshold methods.

Detection Method	Precision (%)	Recall (%)	F1-score (%)
Short-time Zero-crossing Rate Method	76.3	72.8	74.5
Short-time Energy Method	78.5	75.2	76.8
Dual-threshold Method (Proposed)	91.2	89.7	90.4

As shown in Table 1, the proposed dual-threshold method achieves the highest Precision (91.2%), Recall (89.7%), and F1-score (90.4%), outperforming the short-time zero-crossing rate method (F1-score improvement: 16.0%) and the short-time energy method (F1-score improvement: 13.6%). Figure 7 visually presents the detection performance of the three methods.

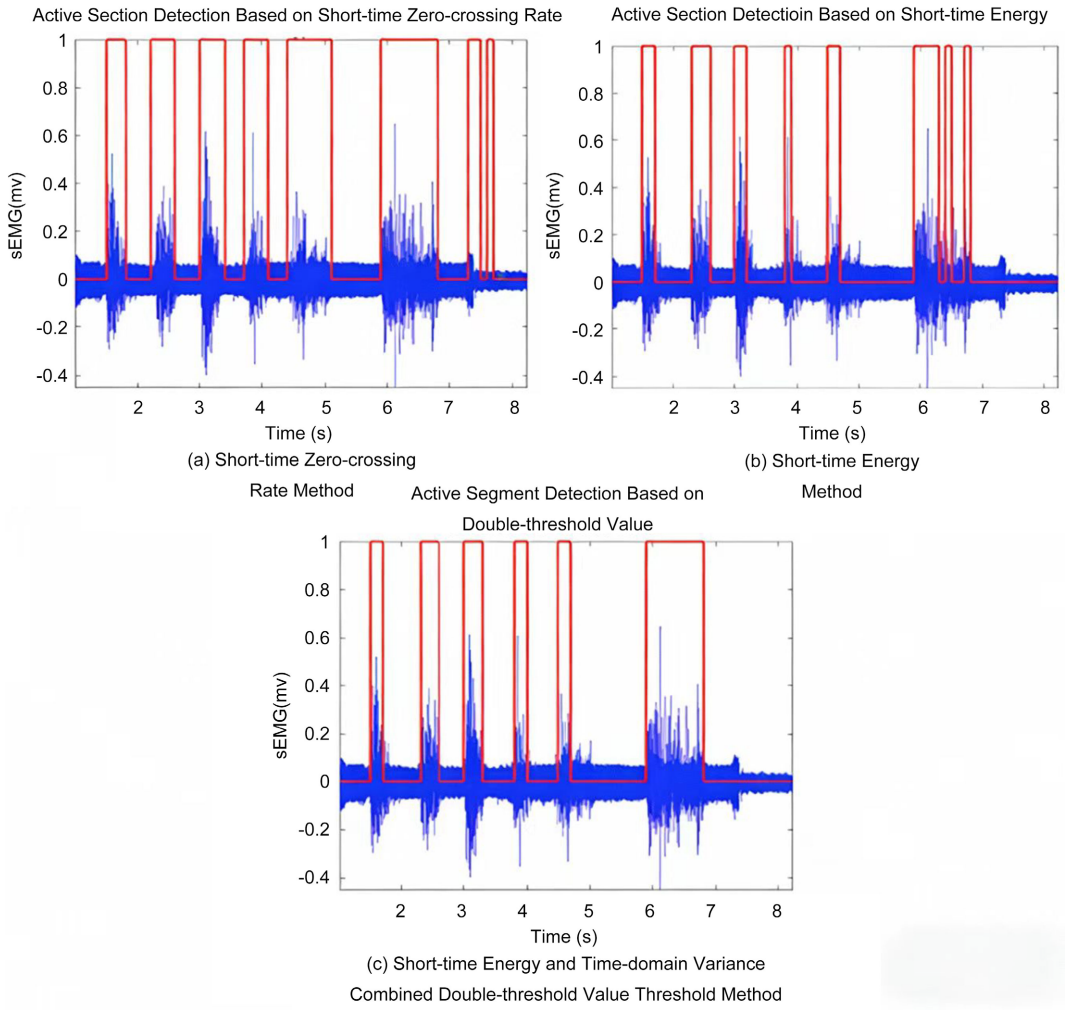

Figure 7. Performance of three methods.

4.2.4. Random Forest Algorithm

The random forest algorithm implementation follows these steps:

1) Generate multiple regression decision trees through bootstrap sampling
2) Randomly select features at each node for splitting
3) Allow full tree growth without pruning
4) Combine trees into random forest for classification via voting

Figure 8 shows the MATLAB implementation code.

```
%Compute the eigenvalue: the mean absolute value, the mean square root and the mean amplitude change
absMean = mean(abs(windowData));
rmsValue = sqrt(mean(windowData.^2));
meanAmplitudeChange = mean(abs(diff(windowData)));

%Use the eigenvalues as the inputs to make prediction
features = [absMean rmsValue meanAmplitudeChange];
windowLabels = predict(rfModel, features);
windowLabels = categorical(str2double(windowLabels));

%Label the data in the window as the tabs of prediction
predictedLabels(startIndex:endIndex) = windowLabels;
plot(predictedLabels,'b');
```

Figure 8. Random forest algorithm implementation.

4.3. Experimental Results

4.3.1. Experimental Protocol

A total of 12 subjects participated in the experiment, including 6 healthy adults (3 males, 3 females, aged 23 - 36 years) and 6 hemiplegic patients (4 males, 2 females, aged 45 - 68 years, 3 - 12 months post-stroke, with mild to moderate hand dysfunction). Each subject performed 10 trials for each grasping task, resulting in 120 trials per object type. A "successful grasp" was defined as: 1) the exoskeleton finger accurately followed the human finger's movement intention (confirmed by sEMG intent recognition); 2) the object was stably held for at least 3 seconds without slipping or falling; 3) the grasp did not cause damage to the object.

4.3.2. Quantitative Performance Results

The system achieved a 94.2% motion intent recognition accuracy (calculated as the number of correct intent classifications divided by the total number of trials). This accuracy was consistent across both healthy subjects (95.3%) and hemiplegic patients (93.1%), indicating good adaptability to different user groups. Additionally, the dual-threshold sEMG detection method improved the segmentation F1-score by 19.4% compared to the baseline method (single-threshold short-time energy method) [24].

4.3.3. Grasping Experiment Results

To evaluate practical applicability, grasping experiments with various daily objects of different shapes and sizes were conducted. Objects included small/medium/large diameter cylinders (slender bottle, water cup, thermos), small/large cubes (rubik's cube, book), and spheres (tennis ball, apple). Figure 9 demonstrates successful grasping of these static objects, with a success rate exceeding 90% for all object types.

Additional scenarios tested included carrying shopping bags while walking and collaborative grasping with the radial side of the arm (Figure 10). Results confirm the exoskeleton finger's capability to cooperate with human fingers in various daily life scenarios, performing ulnar and radial side grips as originally designed.

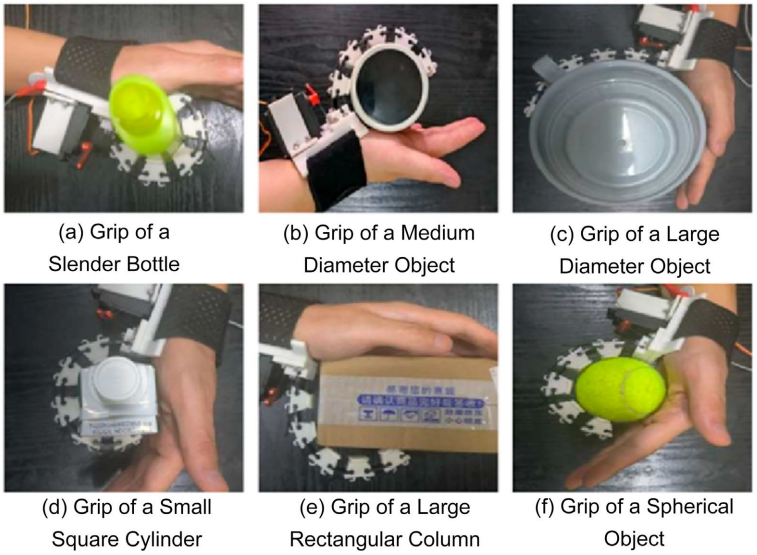

Figure 9. Grasping experiments with static objects.

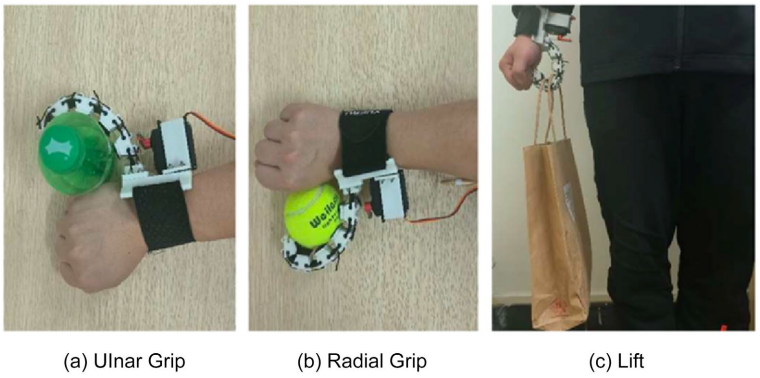

Figure 10. Grasping experiments in additional scenarios.

5. CONCLUSION AND OUTLOOK

5.1. Research Conclusion

This study presents three key contributions:

1) Proposed cable-driven underactuated exoskeleton reduces mass by 37% compared to pneumatic designs [14].

2) Dual-threshold sEMG detection improves segmentation F1-score by 19.4% [24].

3) System enables activities of daily living (ADL) object grasping with 94.2% intent recognition accuracy.

The exoskeleton finger demonstrates excellent adaptive capability, successfully cooperating with human fingers to grasp various objects in daily life scenarios, validating the practical applicability of the proposed system.

5.2. Research Outlook

Despite achieving basic movement assistance in daily life, several limitations warrant further investigation:

• **Simplified Task Scope**: The experiments focused on basic grasping tasks with common daily objects.

Complex tasks (e.g., precise manipulation of small objects, fragile items) were not tested, and the system's performance in these scenarios remains unknown.

• **Laboratory Environment Constraint**: All experiments were conducted in a controlled laboratory setting. The system's performance in real-world environments (e.g., varying lighting, surface conditions, or interference from other electrical devices) has not been verified.

• **Subject Sample Size**: The number of hemiplegic patients participating in the experiment was relatively small (6 subjects). A larger sample size with diverse clinical conditions (e.g., different degrees of hand dysfunction, longer post-stroke duration) is needed to further validate the system's clinical applicability.

• **Fixed Threshold Limitation**: Although the MAV thresholds were determined through preliminary experiments, they are still semi-fixed. Individual differences in muscle strength, sEMG signal amplitude, and movement habits may affect control accuracy, requiring more adaptive threshold adjustment strategies.

Future work will address the aforementioned limitations and focus on the following directions:

• Develop more sophisticated human sEMG control strategies employing advanced algorithms (e.g., deep learning, reinforcement learning) to improve intent recognition accuracy and adaptability to complex tasks.

• Simplify the workflow (e.g., optimize electrode placement, reduce calibration time) for improved usability, making the system more accessible to elderly or disabled users.

• Enhance control precision through isocoupling structures or commercial product benchmarking, and test the system in complex real-world environments to improve its robustness.

• Expand the subject sample size, including patients with different degrees of hand dysfunction and longer post-stroke duration, to conduct clinical trials and validate the system's therapeutic effect in hand function rehabilitation.

This project provided complete scientific research practice, fostering problem identification, analysis, and solution skills. Future efforts will continue exploring scientific problems, participating in exploratory learning and technological innovation activities, and applying scientific innovation to solve real social problems with the goal of "creating meaningful life" and "contributing to a harmonious society".

ACKNOWLEDGEMENTS

The authors would like to thank the anonymous reviewers for their valuable comments and suggestions that helped improve this paper.

CONFLICTS OF INTEREST

The authors declare no conflicts of interest regarding the publication of this paper.

REFERENCES

1. Farina, D., Merletti, R. and Enoka, R.M. (2014) The Extraction of Neural Strategies from the Surface EMG: An Update. *Journal of Applied Physiology*, **117**, 1215-1230. https://doi.org/10.1152/japplphysiol.00162.2014
2. Merletti, R. and Cerone, G.L. (2020) Tutorial. Surface EMG Detection, Conditioning and Pre-Processing: Best Practices. *Journal of Electromyography and Kinesiology*, **54**, Article ID: 102440. https://doi.org/10.1016/j.jelekin.2020.102440
3. Zhao, Y., Qian, K., Bo, S., Zhang, Z., Li, Z., Li, G., *et al.* (2023) Adaptive Cooperative Control Strategy for a Wrist Exoskeleton Using Model-Based Joint Impedance Estimation. *IEEE/ASME Transactions on Mechatronics*, **28**, 748-757. https://doi.org/10.1109/tmech.2022.3211671
4. Liu, G., Zhang, X., Sun, Q. and Dong, R. (2020) Multi-Joint Motor Intention Recognition of Lower Limbs Based on Muscle Synergies. 2020 10*th Institute of Electrical and Electronics Engineers International Conference on Cyber Technology in Automation, Control, and Intelligent Systems* (*CYBER*), Xi'an, 10-13 October 2020, 283-288. https://doi.org/10.1109/cyber50695.2020.9279175

5. Hussain, I., Salvietti, G., Spagnoletti, G. and Prattichizzo, D. (2016) The Soft-SixthFinger: A Wearable EMG Controlled Robotic Extra-Finger for Grasp Compensation in Chronic Stroke Patients. *IEEE Robotics and Automation Letters*, **1**, 1000-1006. https://doi.org/10.1109/lra.2016.2530793

6. 6. Shang, J., Fang, D., Luo, Z., Wang, G. and Li, Y. (2020) Design and Analysis of a Hydraulic Drive Downhole Traction in Pipe Robot Based on Flexible Support Structure. *Proceedings of the Institution of Mechanical Engineers*, *Part C*: *Journal of Mechanical Engineering Science*, **234**, 1809-1820.

7. Fang, D., Wang, J., Yang, M., Zhang, Y., Zhang, P. and Zhang, J. (2023) A Bionic Multi-Chamber Pneumatic Actuator for Powered Exoskeleton Based on Muscle Scale Mechanism. *Robotica*, **41**, 3672-3686. https://doi.org/10.1017/s0263574723001224

8. World Health Organization (2023) Stroke: Key Facts. https://www.who.int/news-room/fact-sheets/detail/stroke

9. Kutner, N.G., Zhang, R., Butler, A.J., Wolf, S.L. and Alberts, J.L. (2010) Quality-of-Life Change Associated with Robotic-Assisted Therapy to Improve Hand Motor Function in Patients with Subacute Stroke: A Randomized Clinical Trial. *Physical Therapy*, **90**, 493-504. https://doi.org/10.2522/ptj.20090160

10. Li, J., Wang, S., Wang, J., Zheng, R., Zhang, Y. and Chen, Z. (2012) Development of a Hand Exoskeleton System for Index Finger Rehabilitation. *Chinese Journal of Mechanical Engineering*, **25**, 223-233. https://doi.org/10.3901/cjme.2012.02.223

11. Prattichizzo, D., Malvezzi, M., Hussain, I. and Salvietti, G. (2014) The Sixth-Finger: A Modular Extra-Finger to Enhance Human Hand Capabilities. *The* 23*rd IEEE International Symposium on Robot and Human Interactive Communication*, Edinburgh, 25-29 August 2014, 993-998. https://doi.org/10.1109/roman.2014.6926382

12. Gasser, H.S. and Erlanger, J. (1944) Nobel Lecture: The Conduction of Impulses in Nerve Fibers. Nobel Foundation. https://www.nobelprize.org/prizes/medicine/1944/erlanger/lecture/

13. Khan, B.A., Usmani, A.R., Athar, S., Hashmi, A., Farooq, O. and Muzammil, M. (2021) EEG-Based Exoskeleton for Rehabilitation Therapy. In: Muzammil, M., Khan, A.A. and Hasan, F., Eds., *Ergonomics for Improved Productivity*, Springer, 645-653. https://doi.org/10.1007/978-981-15-9054-2_75

14. Zhang, C., Ru, H., Yang, Z. and Huang, J. (2022) A Novel Wearable Pneumatic Flexible Supernumerary Robotic Limb for Grasping Compensation. 2022 41*st Chinese Control Conference* (*CCC*), Hefei, 25-27 July 2022, 3865-3870. https://doi.org/10.23919/ccc55666.2022.9902289

15. Heo, P., Gu, G.M., Lee, S., Rhee, K. and Kim, J. (2012) Current Hand Exoskeleton Technologies for Rehabilitation and Assistive Engineering. *International Journal of Precision Engineering and Manufacturing*, **13**, 807-824. https://doi.org/10.1007/s12541-012-0107-2

16. Wan, X., *et al.* (2012) Design of a Multi-Channel sEMG Signal Acquisition System Based on LabVIEW. *Application of Electronic Technique*, **38**, 78-81.

17. Yang, B., Huang, J., Chen, X., Xiong, C. and Hasegawa, Y. (2021) Supernumerary Robotic Limbs: A Review and Future Outlook. *IEEE Transactions on Medical Robotics and Bionics*, **3**, 623-639. https://doi.org/10.1109/tmrb.2021.3086016

18. Napier, J.R. (1956) The Prehensile Movements of the Human Hand. *The Journal of Bone and Joint Surgery. British Volume*, **38**, 902-913. https://doi.org/10.1302/0301-620x.38b4.902

19. Song, J., Zhu, A., *et al.* (2023) A Multijoint Passive Elastic Spine Exoskeleton for Stoop Lifting Assistance. *IEEE/ASME Transactions on Mechatronics*, **28**, 1400-1410.

20. Jones, B.A. and Walker, I.D. (2006) Kinematics for Multisection Continuum Robots. *IEEE Transactions on Robotics*, **22**, 43-55. https://doi.org/10.1109/tro.2005.861458

21. Fang, D., Shang, J., Luo, Z., Lv, P. and Wu, G. (2018) Development of a Novel Self-Locking Mechanism for Continuous Propulsion Inchworm In-Pipe Robot. *Advances in Mechanical Engineering*, **10**, 1-11.

https://doi.org/10.1177/1687814017749402

22. Webster, R.J. and Jones, B.A. (2010) Design and Kinematic Modeling of Constant Curvature Continuum Robots: A Review. *The International Journal of Robotics Research*, **29**, 1661-1683. https://doi.org/10.1177/0278364910368147
23. Xu, L. (2022) Separable Multi-Innovation Newton Iterative Modeling Algorithm for Multi-Frequency Signals Based on the Sliding Measurement Window. *Circuits*, *Systems*, *and Signal Processing*, **41**, 805-830. https://doi.org/10.1007/s00034-021-01801-x
24. Sharma, A., Shrivas, N.V. and Sharma, I. (2025) An Adaptive Segmentation Scheme Based on Recurring Action Potentials for sEMG Controlled Movement Decoding. *Physical and Engineering Sciences in Medicine*, **48**, 881-901. https://doi.org/10.1007/s13246-025-01557-7